Chemistry Europe
European Chemical Societies Publishing

WILEY VCH

Excellence in Chemistry Research

Announcing our new flagship journal

- Gold Open Access
- Publishing charges waived
- Preprints welcome
- Edited by active scientists

Meet the Editors of *ChemistryEurope*

Luisa De Cola
Università degli Studi di Milano Statale, Italy

Ive Hermans
University of Wisconsin-Madison, USA

Ken Tanaka
Tokyo Institute of Technology, Japan

ChemPlusChem

Research Article
doi.org/10.1002/cplu.202300172

Chemistry Europe
European Chemical Societies Publishing

www.chempluschem.org

A Calcination-Free Sol-Gel Method to Prepare TiO_2-Based Hybrid Semiconductors for Enhanced Visible Light-Driven Hydrogen Production

Kang Yang,[a] Dan Wei,[a] Chunman Jia,*[a] and Jianwei Li*[a, b]

In recent years, the sol-gel method has been extensively utilized to develop efficient and stable organic semiconductor composite titanium dioxide (TiO_2) photocatalysts. However, the high-temperature calcination requirements of this method consume energy during preparation and degrade encapsulated organic semiconductor molecules, resulting in decreased photocatalytic hydrogen production efficiency. In this study, we found that by selecting an appropriate organic semiconductor molecule, 1,4-naphthalene dicarboxylic acid (NA), high-temperature calcination can be avoided in the sol-gel process, yielding an organic-inorganic hybrid material with stable and effective photocatalytic properties. The uncalcined material displayed a hydrogen production rate of $2920 \pm 15\ \mu mol\ g^{-1}\ h^{-1}$, which was approximately twice the maximum production rate observed in the calcined material. Likewise, the specific surface area of the uncalcined material, at $252.84\ m^2\ g^{-1}$, was significantly larger compared to the calcined material. Comprehensive analyses confirmed successful NA and TiO_2 doping, while UV-vis and Mott-Schottky tests revealed a reduced energy bandgap (2.1 eV) and expanded light absorption range. Furthermore, the material maintained robust photocatalytic activity after a 40-hour cycle test. Our findings demonstrate that by using NA doping without calcination, excellent hydrogen production performance can be achieved, offering a novel approach for environmentally friendly and energy-saving production of organic semiconductor composite TiO_2 materials.

Introduction

The urgent need for sustainable and eco-friendly energy sources has led researchers to explore innovative materials and methods for hydrogen production.[1] Photocatalytic water splitting, a process that uses sunlight to produce hydrogen from water, offers significant potential for clean and renewable energy generation.[2] Titanium dioxide (TiO_2), a widely studied photocatalyst, has attracted attention due to its non-toxicity, abundance, and excellent photoelectric conversion capabilities.[3] However, the wide bandgap of TiO_2 limits its efficiency in utilizing sunlight, calling for innovative approaches to improve its performance.[4]

The sol-gel method has emerged as a popular technique for synthesizing TiO_2 photocatalysts, as it offers precise control over the material's composition and structure.[5] This process involves the preparation of a titanium precursor, hydrolysis, condensation, gelation, aging, drying, and finally calcination, resulting in crystalline TiO_2.[6] However, traditional sol-gel methods often require high-temperature calcination, which can be energy-intensive and not in line with current green development goals.[7]

In this research, a green and energy-efficient strategy for synthesizing TiO_2 and organic semiconductor hybrid materials using a low-temperature sol-gel method is presented. The choice of 1,4-naphthalene dicarboxylic acid (NA) as an organic semiconductor is motivated by its π-π stacking effect, produced by a stable conjugated large π system on the naphthalene structure, which is conducive to electron transport.[8] Furthermore, the carboxyl functional group (−COOH) of the NA generates hydrogen bonds and π-π interactions between molecules.[9] This innovative technique effectively addresses the limitations associated with conventional high-temperature calcination processes.

Using tetrabutyl titanate ($Ti(OC_4H_9)_4$) as the titanium source at lower temperatures (25-60 °C), the simple sol-gel method with a small quantity of NA (2.5 wt%) for organic-inorganic hybridization eliminates the need for high-temperature calcination, yielding a photocatalytic material with an impressive hydrogen production rate and stable cycle performance under visible light.

This research establishes a pioneering method for modifying TiO_2's structure by decreasing its bandgap width, augmenting its visible light absorption range, and substantially enhancing its electron transport rate in the hybrid material. The successful synthesis of NA–TiO_2 (2.5 wt%) exemplifies the potential of this approach for mass production of photocatalytic materials.

[a] K. Yang, D. Wei, Prof. C. Jia, Dr. J. Li
School of Chemical Engineering and Technology
Hainan University
Haikou 570228, China
E-mail: jiachunman@hainanu.edu.cn
[b] Dr. J. Li
MediCity Research Laboratory
University of Turku
Tykistökatu 6, FI-20520 Turku, Finland
E-mail: jianwei.li@utu.fi

Supporting information for this article is available on the WWW under https://doi.org/10.1002/cplu.202300172

Moreover, the identification of a stable ester bond (Ti–O-C=O) within the NA–TiO_2 (2.5 wt%) material and the increased specific surface area attained without high-temperature calcination contribute to the novelty of this study. These breakthroughs lay the groundwork for novel strategies and concepts in the development of eco-friendly, energy-efficient organic semiconductor hybrid TiO_2 photocatalytic materials, presenting promising applications across various industries pursuing green and sustainable energy solutions.

Results and Discussion

Characterization of materials

The synthetic procedures of the TiO_2 materials hybridized with the NA has been presented in the Experimental section. The name of the resulting material is noted as NA–TiO_2 (n wt%), when the weight percentage of NA was n%. To analyze the crystal phase relationship of the compound NA-doped material NA–TiO_2, Powder X-Ray Diffraction (PXRD) was employed for spectral analysis. As illustrated in Figure 1A and S2, the positions at 25.28°, 37.80°, 48.05°, and 53.89° correspond to the (101), (103), (200), and (204) crystal planes, respectively.[10] The measured crystal planes of NA–TiO_2 were consistent with those of anatase TiO_2, indicating that the crystallization degree of NA–TiO_2 formed through the hybridization process was similar to that of anatase TiO_2.

The morphology and Pt loading of the hybrid material NA–TiO_2 (2.5 wt%) were analyzed using scanning electron microscope (SEM) and Transmission Electron Microscope (TEM). The obtained SEM (Figure S3) and TEM (Figure 1) images of NA–TiO_2 (2.5 wt%) and Pt(0.3 wt%)/NA–TiO_2 (2.5 wt%) materials showed that the TiO_2 particle size was approximately 10 nm (Figure S3 A and S3B). Selected area electron diffraction (SAED) results confirmed the polycrystalline nature of nano-TiO_2 in hybrid materials (Figure 1C). Under full light, K_2PtCl_4 was reduced by methanol, resulting in the formation of Pt (0.3 wt%) nanoparticles supported on the catalyst material's surface. TEM images reveal that the distribution of Pt particles on the surface of the NA–TiO_2 (2.5 wt%) material was uniform, with an approximate size of 3 nm (Figure 1E). As shown in High Resolution Transmission Electron Microscope (HRTEM) (Figure 1F), the lattice spacing of Pt nanoparticles was 0.196 nm, corresponding to the Pt (200) plane, consistent with the crystal plane of Pt particles.[10d,11] Moreover, High-Angle Annular Dark Field (HAADF) (Figure 1G) elemental mapping demonstrated that Ti, O, C, and Pt elements were evenly distributed throughout the hybrid material Pt (0.3 wt%)/NA < C- < TiO_2 (2.5 wt%).

To analyze the impact of calcination on the pore structure and specific surface area of hybrid materials, nitrogen adsorption-desorption isotherms, pore size distribution, and Brunauer-Emmett-Teller (BET) measurements were conducted on NA–TiO_2 and NA–TiO_2 (2.5 wt%) hybrid materials with different NA contents, under high-purity N_2 gas at 77 K. The results, depicted in Figure 2A, 2B, S4, S5 and Tables 1, S1, show that when the doping amount was 2.5 wt%, the BET value was 252.84 $m^2 g^{-1}$ (pore size 4.42 nm), which was significantly larger than that of pristine TiO_2 (179.25 $m^2 g^{-1}$), 0.5 wt% (222.59 $m^2 g^{-1}$), and

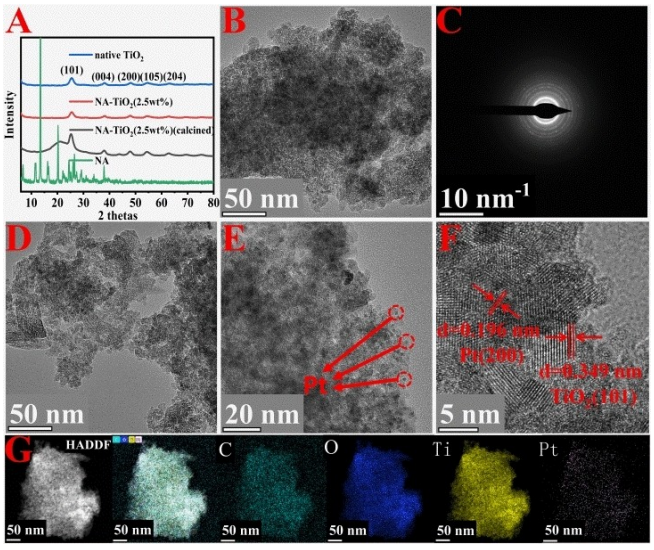

Figure 1. (A) X-ray diffraction pattern of NA–TiO_2 before and after calcination; (B) TEM plot of NA–TiO_2 (2.5 wt%); (C) SAED diagram; (D) and (E) Pt(0.3 wt%)/NA–TiO_2 (2.5 wt%) TEM diagram, (F) HRTEM diagram, (G) element mapping diagram.

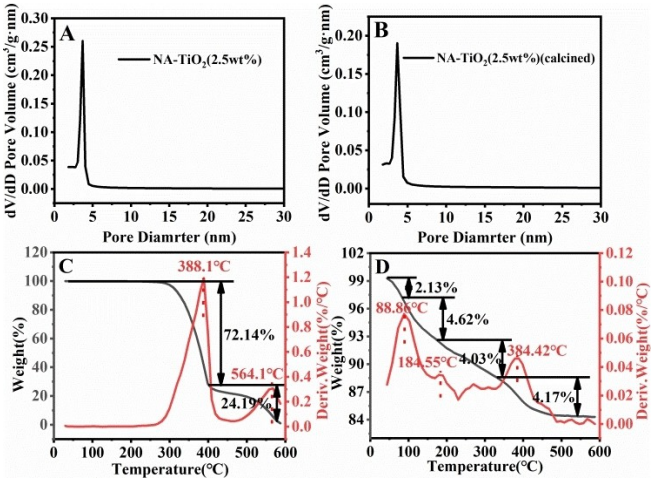

Figure 2. Pore size distribution of NA–TiO_2 (2.5 wt%) (A) before and (B) after calcination; Thermal stability analysis of (C) NA and (D) NA–TiO_2 (2.5 wt%) hybrid materials. Measurements are performed from room temperature to 600 °C at a heating rate of 10 °C/min.

Table 1. Specific surface area, pore size and pore volume of NA–TiO_2 (2.5 wt%) before and after calcination on a 77 K adsorption isotherm.

Sample	Surface area (m2/g)	Pore size (nm)	Pore volume (cm3/g)
native TiO2	179.25	6.13	0.275
NA–TiO2 (2.5 wt%) (calcined)	222.73	4.97	0.278
NA–TiO2 (2.5 wt%)	252.84	4.42	0.264

4.5 wt% (248.58 $m^2 g^{-1}$) samples (Table S1). This increase could be attributed to the dopant's reduction of pores during the synthesis process, which gradually increased the catalyst's specific surface area.[10d,12]

Additionally, the BET value of NA–TiO_2 (2.5 wt%) before calcination was as high as 252.84 $m^2 g^{-1}$ (pore size 4.42 nm), which was significantly higher than the 222.73 $m^2 g^{-1}$ (pore size 4.97 nm) value obtained after calcination. This difference was likely due to the increase in pore size distribution resulting from decomposition induced by high-temperature calcination, as demonstrated in Figure 2A, 2B and Table 1. The mesoporous structure (2.1–5.2 nm) of the NA–TiO_2 material was evident in the pore size distribution diagram, indicating that the NA–TiO_2 prepared using a simple sol-gel method possesses a distinct mesoporous layered structure.[13] This structure helps to enhance the material's porosity, increased the specific surface area, and facilitated better contact between the catalyst and substrate, ultimately improving photocatalytic performance.

To examine the combination of NA and native TiO_2 in the synthesized hybrid material NA–TiO_2, the materials NA, native-TiO_2, NA–TiO_2 (calcined), and NA–TiO_2 were measured using FT-IR spectroscopy. As depicted in Figure S6, a strong broad peak appears between 500–800 cm^{-1} in native TiO_2, which was attributed to the characteristic broad peak of the anatase Ti-O–Ti bond's stretching vibration. The peaks at 3422 cm^{-1} and 1637 cm^{-1} correspond to the stretching and bending vibrations of –OH in water molecules adsorbed on the TiO_2 surface. NA exhibits a strong absorption peak at 1685 cm^{-1}, attributed to the stretching vibration of C=O in NA materials.[14]

In the hybrid material NA–TiO_2, the peak at 3422 cm^{-1} corresponds to the stretching vibration of the -OH bond in the adsorbed H_2O on the material's surface, and the absorption peak at 500–800 cm^{-1} was related to the Ti–O–Ti stretching vibration in NA–TiO_2. Additionally, new absorption peaks at 1625 cm^{-1} and 1412 cm^{-1}, distinct from the peaks of NA and TiO_2 emerge. The peak at 1685 cm^{-1} in the NA material disappears, so the new peaks can be attributed to the emergence of symmetric and asymmetric vibrational peaks different from COO- in NA within the composite. The absorption peak at 1508 cm^{-1} was assigned to the symmetric stretching vibration of C=C. The formation of a new chemical bond, Ti–O–C=O, between the material NA and native TiO_2 can be confirmed by considering the hybrid material sol-gel process.[15] This bond resulted in a strong covalent bond interaction between the two materials, broadening the absorption band of native TiO_2 and effectively improving the hybrid material's performance in producing H_2 by light.

To investigate the hybridization mode and chemical bond state of the hybrid materials Pt(0.3 wt%)/NA–TiO_2(2.5 wt%) and NA–TiO_2(2.5 wt%) before and after calcination, native-TiO_2, NA–TiO_2(2.5 wt%), and Pt(0.3 wt%)/NA–TiO_2(2.5 wt%) were analyzed using X-ray photoelectron spectroscopy (Figure S7, S8, S9 and S10). Typically, with the C 1s peak's binding energy at 284.8 eV (carbon-containing contaminants) as a reference, the binding energies at 286.2 eV and 288.7 eV corresponded to C–O bonds and C=O bonds, respectively (Figure S10 A). The binding energy of O 1s at 529.6 eV was attributed to the Ti–O bond, and the binding energy at 531.4 eV was attributed to surface-OH or C–O bonds (Figure S10B). The binding energies at 458.5 eV and 464.2 eV in Ti 2p were assigned to Ti $2p_{3/2}$ and Ti $2p_{1/2}$, respectively. These results were consistent with the native TiO_2 test results (Figure S7), further confirming the infrared tests (Figure S6) and indicating the formation of a new chemical bond Ti–O-C=O in the hybrid material NA–TiO_2. In the Pt(0.3 wt%)/NA–TiO_2(2.5 wt%) material, binding energies corresponding to 71.70 eV and 75.1 eV were attributed to Pt $4f_{7/2}$ and Pt $4f_{5/2}$ peaks, respectively, representing the formation of Pt(0). New peaks appeared at 72.7 eV and 76.5 eV due to the presence of a small amount of unreduced Pt(II) in K_2PtCl_4 (Figure S10D).[10b,c]

To further understand the thermal stability of the organic compound NA in the hybrid material during high-temperature calcination, NA and NA–TiO_2 (2.5 wt%) were analyzed (Figure 2C and 2D) using a thermogravimetric analyzer and heating from room temperature to 600 °C at a heating rate of 10 °C/min. The results show that NA maintained good thermal stability in the temperature range of 100–300 °C, with no significant mass loss. However, significant mass loss took place in the range of 300–400 °C, attributed to the decomposition of compound NA, reaching a maximum decomposition rate at 388 °C. The decomposition rate was relatively slow between 400–500 °C and started to increase after exceeding 500 °C, reaching the maximum at 564 °C. In the thermogravimetric analysis of the hybrid material NA–TiO_2 (2.5 wt%), a small mass loss (2.13%) in the range of 0–100 °C was attributed to the evaporation of adsorbed water molecules. The 4.62% mass loss in the 100–170 °C range may be due to the volatilization of the DMF solvent used in the sol-gel synthesis process. The larger mass loss beyond 200 °C may be caused by the destruction of the hybrid material's porous structure. The hybrid material started to decompose at temperatures above 300 °C, with the decomposition rate reaching its maximum at 384 °C. This further explained the decrease in hydrogen production performance for calcined NA–TiO_2 (2.5 wt%), while the performance of the uncalcined material was significantly higher than that of the calcined material.[16]

To evaluate the possible hydrogen production ability of the hybrid material NA–TiO_2(2.5 wt%), energy band gap calculations and Mott-Schottky tests were performed on the native-TiO_2 and NA–TiO_2(2.5 wt%) materials (Figure 3B, 3 C and 3D). In the ultraviolet-visible region, the solid-state UV-Vis diffraction spectra of materials NA, native-TiO_2, and NA–TiO_2(2.5 wt%) were measured (Figure 3A). Native-TiO_2 showed no absorption in the visible region, with only a strong absorption peak at 320 nm. Organic NA exhibited weak absorption at wavelengths of 420–400 nm, while the hybrid material NA–TiO_2(2.5 wt%) displayed a broad absorption band at 400–600 nm. The light absorption of native-TiO_2 was extended to the visible light range through organic doping, significantly enhancing its absorption capacity. This improvement is attributed to the presence of Ti–O-C=O bonds in the NA–TiO_2(2.5 wt%) material, which enabled native-TiO_2 to absorb visible light (Figure S6).[17]

The energy band diagram of native TiO_2 showed a single band gap of 3.2 eV, whereas the hybrid material

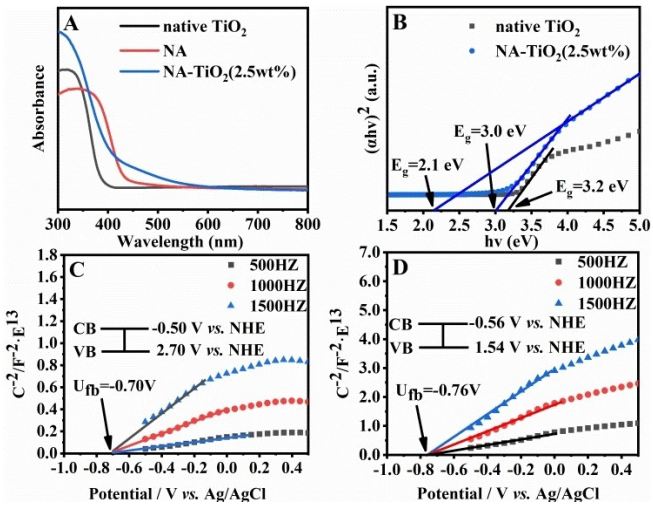

Figure 3. (A) UV-Vis spectra of native-TiO_2, NA and NA–TiO_2 (2.5 wt%); (B) bandgap plots for NA–TiO_2 (2.5 wt%) and native-TiO_2; (C) Mott-SChottky plots for native-TiO_2; (D) Mott-SChottky plot for NA–TiO_2 (2.5 wt%).

NA–TiO_2(2.5 wt%) displayed two distinct band gaps: a narrow band gap of 2.1 eV, corresponding to visible region absorption, and a wide band gap of 3.0 eV, corresponding to ultraviolet region absorption (Figure S11). The formation of Ti–O-C=O in the hybrid material reduced the band gap of native TiO_2, effectively decreasing electron-hole recombination to capture photogenerated electrons and enhancing the photocatalytic hydrogen production.[10d,11b]

The Mott-Schottky test of the material confirmed the feasibility of subsequent photocatalytic hydrogen production. As shown in Figure 3C and 3D, the flat band points of native-TiO_2 and NA–TiO_2(2.5 wt%) are −0.70 V and −0.76 V, respectively. The flat band potentials for native-TiO_2 and NA–TiO_2 are −0.50 V and −0.56 V, respectively. These values correspond to the conduction band potentials (vs. NHE) of native-TiO_2 and NA–TiO_2(2.5 wt%), which are more negative than the reduction potential (0 V) of H^+/H_2. Additionally, the conduction bands of native-TiO_2 and NA–TiO_2 were calculated from UV-vis measurements to be 2.70 V and 1.54 V (vs. NHE), respectively. The more negative conduction band potential of NA–TiO_2(2.5 wt%) confirmed its ability to produce hydrogen effectively.[10d]

Photocatalytic hydrogen production performance

The use of NA-doped native-TiO_2 successfully extended the absorption range of NA–TiO_2 to visible light and reduced the bandgap width. Additionally, Pt has a larger work function, making it more conducive to photocatalytic hydrogen production. Therefore, we used Pt (0.3 wt%) to support NA–TiO_2 and evaluated their hydrogen production performance under visible light using triethanolamine (TEOA) as a sacrificial agent.[10d,18]

To determine the optimal hybrid material for hydrogen production, we tested NA–TiO_2 (0.5 wt%), NA–TiO_2 (2.5 wt%), and NA–TiO_2 (4.5 wt%) for 5 hours. The results showed that the 2.5 wt% doped hybrid material exhibited the best hydrogen production performance. The hydrogen production performance of NA–TiO_2 is related to the dopant content. When the content was too low, native TiO_2's light absorption range could not effectively extend to the ultraviolet region. When the content was too high, the hybrid material's pore size increased and the specific surface area decreased, affecting photocatalytic performance (Figure S12).

We calcined NA–TiO_2 (2.5 wt%) at high temperature at calcination rates of 5 °C/min and 2.5 °C/min under air atmosphere, and determined the hydrogen production performance of NA–TiO_2 (2.5 wt%) before and after calcination for 5 h. The photocatalytic hydrogen production rate of uncalcined NA–TiO_2 (2.5 wt%) was $2920 \pm 15\ \mu mol\ g^{-1}\ h^{-1}$, significantly higher than the maximum rate ($1646 \pm 10\ \mu mol\ g^{-1}\ h^{-1}$) of calcined material, which further confirmed that high-temperature calcination destroyed the pore structure of the material, resulting in reduced hydrogen production performance (Figure 4A and S13).

To select the best metal co-catalyst, we tested Cu, Ni, and Pt for photocatalytic hydrogen production performance. Pt-(0.3 wt%)/ NA–TiO_2(2.5 wt%) exhibited a strong photocatalytic hydrogen production performance from water, much higher than that of Cu (0.3 wt%) / NA–TiO_2 (2.5 wt%) and Ni (0.3 wt%)/NA–TiO_2 (2.5 wt%) (Figure S14).[19] This is because Pt maximizes the photocatalyst's catalytic activity, increasing the electron transfer rate, effectively absorbing the photogenerated charge on the photocatalyst, promoting charge separation, and allowing the separated charge to participate in redox reactions. Based on this, we loaded different amounts of Pt onto NA–TiO_2 (2.5 wt%) to study the material's hydrogen production performance. The results showed that a small amount of Pt loading significantly increased hydrogen production performance (Fig-

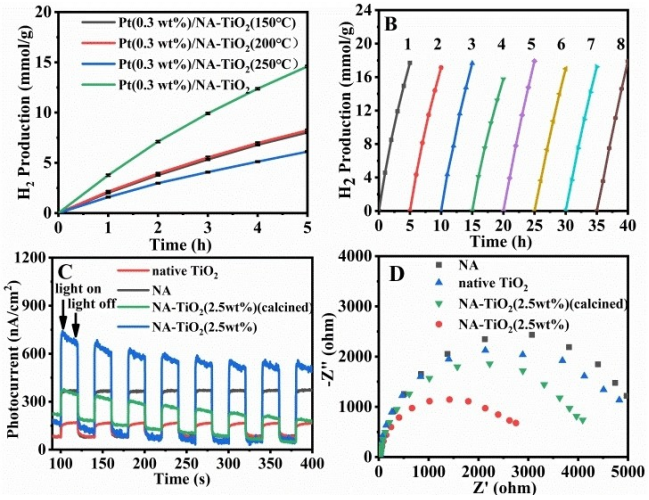

Figure 4. (A) Effect of calcination temperature on hydrogen production performance of NA–TiO_2 material in 20 mL water/triethanolamine solution (9:1 volume ratio) under visible light ($\lambda > 400$ nm); (B) Stability test of Pt(0.3 wt%)/NA–TiO_2 (2.5 wt%), photocatalytic hydrogen production cycle under visible light ($\lambda > 400$ nm); (C) Instantaneous current response of native TiO_2 (red line), NA (black line), NA–TiO_2 (2.5 wt%) (calcined) (green line) and NA–TiO_2 (2.5 wt%) (blue line); (D) Electrochemical impedance plots of NA (black square), native TiO_2 (blue upper triangle), NA–TiO_2 (2.5 wt%) (calcined) (green triangle), and NA–TiO_2 (2.5 wt%) (red circle).

ure S15).[20] In addition, compared with various reported photocatalysts for hydrogen production, the NA–TiO_2 also showed excellent efficiency (see Table S5).

Inductively Coupled Plasma Atomic Emission Spectroscopy (ICP-AES) analysis was carried out on different loading contents of Pt to further understand the loading of Pt nanoparticles on the surface of NA–TiO_2 (2.5 wt%) material, confirming that the Pt NPs were successfully loaded onto the material's surface (Table S2).

To verify the stability and repeatability of the hybrid material NA–TiO_2 (2.5 wt%), a cycle stability experiment was conducted, demonstrating that the material maintained high activity after 40 hours (Figure 4B). The turnover numbers (TON) H_2 calculated after the 40-hour cycle experiment reached 8988, showing that low Pt content could effectively produce extremely high hydrogen with high energy use value. The results of hydrogen production indicated a good correspondence between the absorption wavelength range of NA–TiO_2 (2.5 wt%) and the amount of hydrogen produced, further suggesting that hydrogen generation was highly related to the hybrid material's absorption range (Table S3).

To further verify the photoelectric response ability of NA–TiO_2 (2.5 wt%), we conducted electrochemical tests on native TiO_2, NA, NA–TiO_2 (2.5 wt%) (calcined), and NA–TiO_2 (2.5 wt%) using a three-electrode battery system. We obtained photocurrent-time (I-t) curves for these materials under on/off illumination and recorded their photocurrent response spectra (Figure 4C). The results confirmed that uncalcined NA–TiO_2 (2.5 wt%) has a stronger photo-responsive ability. In the measured electrochemical impedance spectroscopy (EIS) (Figure 4D), the arc radius of NA–TiO_2 (2.5 wt%) was smaller than that of NA–TiO_2 (2.5 wt%) (calcined), indicating lower carrier transfer resistance and faster interface carrier transfer for NA–TiO_2 (2.5 wt%). This property is more conducive to electron transport and higher photocatalytic activity.

We performed ICP-AE, XRD, and XPS tests on Pt (0.3 wt%)/NA–TiO_2 (2.5 wt%) (Table S4, Figure S16 and S17) to further study the stability of the material's structure and composition after 40 hours of cycling, and the content of the supported Pt. The results showed that after 40 hours of cyclic hydrogen production testing, the material still contained 0.0434 wt% Pt. This finding proves that Pt (0.3 wt%)/NA–TiO_2 (2.5 wt%) can effectively deposit Pt nanoparticles on the surface, enabling the hybrid material to be reused and indicating its stability.

The XRD results demonstrated that the material maintained high crystallinity after cycling, which positively impacts the cycle activity of the NA–TiO_2 (2.5 wt%) catalyst. This finding further illustrates that the material's crystallinity did not change with the number of cycles but could consistently promote the generation and transfer of photogenerated carriers, which was why NA–TiO_2 (2.5 wt%) can cycle stably. These results were also consistent with the pre-cycling test results (Figure 1A). XPS analysis showed that the binding energy of the C 1s peak at 284.8 eV was used as a reference for carbon-containing pollutants, and the binding energies corresponding to 71.6 eV and 74.9 eV were attributed to the peaks of Pt $4f_{7/2}$ and Pt $4f_{5/2}$, respectively. The chemical bond state of Pt(0) was consistent with that before the cycle, indicating that Pt (0.3 wt%)/NA–TiO_2 (2.5 wt%) exhibited remarkable hydrogen production stability and reusability.

Study on photocatalytic mechanism

To investigate the internal mechanism of photocatalytic hydrogen production for the hybrid material Pt(0.3 wt%)/NA–TiO_2 (2.5 wt%), we conducted solid-state fluorescence tests on hybrid materials with different doping amounts and before and after calcination. The results revealed that the fluorescence emission spectrum peak of NA–TiO_2 (2.5 wt%) was the lowest. The other materials followed the order of fluorescence TiO_2 > NA–TiO_2 (4.5 wt%) > NA–TiO_2 (0.5 wt%) > NA–TiO_2 (2.5 wt%) (calcined) > NA–TiO_2 (2.5 wt%) (Figure S18). This indicated that materials with stronger fluorescence intensity absorb energy, which was then excited in the form of fluorescence.[10d,21] This process led to rapid recombination of electrons and holes, resulting in a significant reduction in photocatalytic hydrogen production ability. These findings demonstrated that NA–TiO_2 (2.5 wt%) had strong photocatalytic performance.

Through FT-IR and XPS analyses of the hybrid material NA–TiO_2 (2.5 wt%), it can be reasonably confirmed that the organic semiconductor NA and native TiO_2 can be stably combined without high-temperature calcination (Figure 5). The valence bond Ti–O-C=O connected the two materials, and the bandgap of native TiO_2 was successfully reduced by NA hybridization, as evidenced by UV-vis and Mott-Schottky tests. This significantly improved the absorption wavelength range of native TiO_2, extending its absorption from the ultraviolet region to the visible region. During the photocatalytic hydrogen production process, photoexcitation facilitates the separation of electrons and holes in the hybrid material NA–TiO_2 (2.5 wt%). The generated electrons could be easily transferred to the Pt nanoparticles on the material's surface for redox reactions. This efficient charge transport ability enabled rapid hydrogen production from water splitting.[22]

In order to further elucidate the photocatalytic mechanism, the main active radicals (·OH and $O_2{\cdot}^-$) in the Pt(0.3 wt%)/

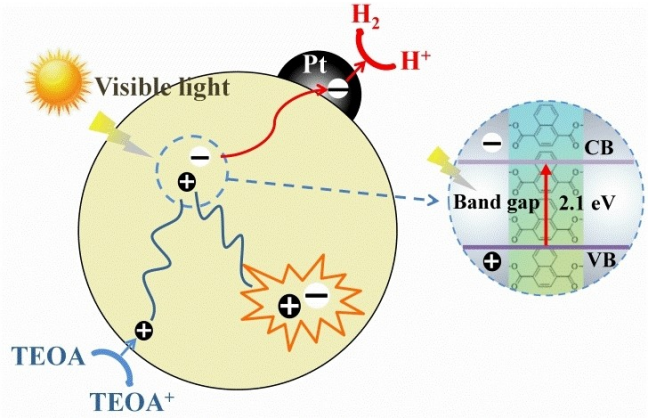

Figure 5. Hydrogen production mechanism of NA–TiO_2 (2.5 wt%).

NA–TiO_2(2.5 wt%) photocatalytic reaction system were detected by quenching experiments. Isopropanol (IPA 100 mM) and benzoquinone (BQ, 1 mM) were used as quenchers for hydroxyl radicals (·OH) and superoxide ($O_2{\cdot}^-$). As shown in Figure S19, the hydrogen production decreased by 23% and 71% relative to that without the addition of quencher, which was attributed to ·OH and $O_2{\cdot}^-$, respectively. Among them, the influence of OH was negligible, while $O_2{\cdot}^-$ played significant roles in the photocatalytic reaction process. The reactive species were identified by electron spin resonance (EPR). As shown in Figure S20 and S21, DMPO-$O_2{\cdot}^-$ and DMPO-·OH were performed under dark and visible light irradiation for 10 min. The material Pt(0.3 wt%)/NA–TiO_2 (2.5 wt%) was effective during the irradiation, as both ·OH and $O_2{\cdot}^-$ had detectable signals. However, when the lamp was off, no signal was detected. Theoretically, there should be no ·OH generation due to the more negative valence band of NA–TiO_2 (2.5 wt%) (1.56 eV vs. NHE) than ·OH ($E_0(\cdot OH/H_2O) = 2.27$ eV vs. NHE. Thus, the detected ·OH should be attributed to the conversion of $O_2{\cdot}^-$. In addition, in the Mott-Schottky test plot (Figure 3D), the CB (−0.56 eV) of NA–TiO_2(2.5 wt%) was more negative than $E_0(O_2/O_2{\cdot}^-)$ (−0.33 eV), which suggested that electrons could react with O_2 to form O2·$^-$.[23] All together, we proposed the mechanism in the following steps:

$$Pt(0.3\ wt\%)/NA{-}TiO_2(2.5\ wt\%) + h\nu \rightarrow e^- + h^+$$

$$2H_2O + 4\,h^+ \rightarrow O_2 + 4H^+$$

$$O_2 + e^- \rightarrow O_2{\cdot}^-$$

$$O_2{\cdot}^- + e^- + 2H^+ \rightarrow \cdot OH + \cdot OH$$

$$2H^+ + 2e^- \rightarrow H_2$$

Conclusion

By the simple sol-gel method, high-temperature calcination was not required, and only 2.5 wt% of NA was used to successfully prepare the hybrid material NA–TiO_2 (2.5 wt%), which had the characteristics of good stability, high specific surface area, small porosity and mesopores. Under visible light irradiation, the uncalcined NA–TiO_2 (2.5 wt%) material exhibited a photocatalytic hydrogen production efficiency of up to 2920 ± 15 μmol g^{-1} h^{-1}, which was much higher than that of pure TiO_2 and calcined NA–TiO_2 (2.5 wt%). Comprehensive analysis of XRD, FT-IR, XPS, ICP-AES and UV-vis showed that the compound NA was connected to TiO_2 in the form of covalent bond Ti–O–C=O, which effectively reduced the band gap of TiO_2, expanded the light absorption range of hybrid materials to the visible light region, greatly improved the photocatalytic performance, and the photocatalytic activity of NA–TiO_2 (2.5 wt%) was enhanced due to the strong absorption of organic semiconductors in the visible light range. Efficient electron transfer and the formation of stable Ti–O–C=O bonds between compounds NA and TiO_2. This work provides a new way to construct a new photocatalytic hybrid material with low energy consumption and high output value.

Experimental Section

Materials

All chemical reagents used in the experiments were of chromatographic purity and required no further purification. tetrabutyl titanate ($Ti(OC_4H_9)_4$, ≥99.0%), acetic acid (CH_3COOH, ≥99.5%), *N,N*-dimethylformamide (DMF, 99.9%), triethanolamine (TEOA, >99.0%), anhydrous methanol (MeOH, >99.0%), anhydrous ethanol (EtOH, 99.5%), Isopropyl alcohol (IPA >99.0%), benzoquinone (BQ, >99.0%) and 1,4-naphthalene dicarboxylic acid (NA, 98%) were obtained from Innochem (Beijing, China).

Synthesis of NA- TiO_2 composites

The hybrid material NA–TiO_2 is presented in Figure S1 and prepared using a straightforward sol-gel method with varying contents. The preparation process (conducted at room temperature) involves the following steps: First, mix 1 mL of DMF, 168 μL of glacial acetic acid, and 106 μL of ultrapure water in a 20 mL sample bottle and stir for 2 minutes until fully combined, resulting in a colorless and transparent solution. Then, quickly add 1 mL of tetrabutyl titanate, followed by 1.25 mg, 6.25 mg, and 11.25 mg of compound 1,4-naphthalene dicarboxylic acid, stirring vigorously for 5 minutes to achieve a homogeneous mixture. The solution becomes yellow and transparent at this stage. Finally, gradually increase the temperature from 45 °C to 60 °C, causing the solution to become gel-like. Dry the sample in a 60 °C oven for 12 hours. After complete drying, extract the product with water for 48 hours, yielding light yellow solids of NA–TiO_2 (0.5 wt%), NA–TiO_2 (2.5 wt%), and NA–TiO_2 (0.45 wt%) hybrid materials.

Synthesis of Pt@NA–TiO_2 composites

Place 20 mg of NA–TiO_2 (2.5 wt%) hybrid material in a transparent glass reactor, and sequentially add 10 mL of H_2O and 8 mL of anhydrous methanol, stirring well. Then, add 30 μL, 60 μL, 90 μL, 120 μL, and 150 μL of potassium tetrachloroplatinate (K_2PtCl_4) and irradiate under a 300 W xenon lamp for 1 hour to obtain a brown-yellow homogeneous suspension (composite material containing Pt nanoparticles). Centrifuge the suspension with H_2O and ethanol for 2 minutes each, yielding brown-yellow Pt(0.15 wt%)@NA–TiO_2 (2.5 wt%), Pt(0.3 wt%)NA–TiO_2 (2.5 wt%), Pt(0.45 wt%)NA–TiO_2 (2.5 wt%), Pt(0.6 wt%)NA–TiO_2 (2.5 wt%), and Pt(0.75 wt%)NA–TiO_2 (2.5 wt%) composite materials.

Hydrogen production by photolysis of water

In the experiment, a Labsolar-6 A photocatalytic analysis system was used for water photolysis to produce hydrogen under vacuum, while a GC9790Plus gas chromatograph was employed to analyze the hydrogen production, allowing for the measurement of the hybrid material's photocatalytic performance. The specific experimental process included the following steps:

1) Weigh 20 mg of the hybrid material Pt@NA–TiO2 (2.5 wt%) in a transparent glass reactor, then weigh 20 mL of triethanolamine (10 vol%) aqueous solution, mix well and stir evenly.
2) Illuminated with a 300 W xenon lamp and experimented with a 400 nm filter.

3) Collect samples every hour and monitor hydrogen production, recording the data accordingly.

Instruments and methods

Scanning electron microscopy (SEM) images of hybrid materials were obtained using a Thermo Scientific Verios G4 UC field emission SEM. Transmission electron microscopy (TEM), high-resolution TEM (HRTEM), and energy-dispersive X-ray spectroscopy (EDX) of the samples were performed with a JEM-2100F TEM at 200 kV. Physical adsorption and desorption tests were conducted using an ASAP 2460 instrument under high-purity N_2 gas at 77 K, with a degassing temperature of 200 °C and degassing time of 10 h. Specific surface area was calculated using the Brunauer-Emmett-Teller (BET) method, and ultra-high purity grade gases were used.

Powder X-ray diffraction (PXRD) tests were carried out on a Rigaku Smart Lab diffractometer (Bragg–Brentano geometry, Cu–Kα1 radiation, $\lambda = 1.54056$ Å). Fourier transform infrared spectroscopy (FT-IR) measurements were performed on a Nicolet iS50 spectrometer (spectral range 4000–500 cm^{-1}, averaging 64 scans). X-ray photoelectron spectroscopy (XPS) was conducted using a Thermo Fisher Scientific K-Alpha+ instrument with an Al Kα X-ray source ($h\nu = 1486.6$ eV) and a 650 μm spot.

Thermal analysis (TGA) was performed using a TAQ600 thermal analyzer under air conditions, with a temperature range between room temperature and 600 °C and a heating rate of 10 °C min^{-1}. The Pt nanoparticle content of the samples was determined using an Agilent ICP-OES730 inductively coupled plasma atomic emission spectrometer (ICP-AES). Solid-state UV-vis absorption spectra were measured with a Shimadzu-2600 spectrometer.

The Mott-Schottky curve was tested using an IVIUMnSTAT electrochemical analyzer in a three-electrode cell, with the sample as the working electrode, an Ag/AgCl electrode as the reference electrode, and a platinum sheet as the counter electrode. The electrolyte was a 0.25 M Na_2SO_4 solution. The sample (2 mg) was dispersed in 1 mL of methanol, mixed with 0.05 mL of Nafion, and sonicated for 30 min. A 50 μL drop was deposited onto FTO conductive glass, forming a film with an area of 0.25 cm^2.

Photocurrent response (I-t) and electrochemical impedance (EIS) tests were performed using three electrodes and a 0.25 M Na_2SO_4 electrolyte solution, with a 300 W xenon lamp and a 400 nm filter as the light source. The hydrogen production system used in the photocatalytic test was Perfect Light Lab Solar-6 A, and hydrogen output was measured with a Fuli 9790II gas chromatograph. Apparent quantum yield (AQY) measurements utilized a Zolix MLED4-1 with incident wavelengths of 405 nm and 450 nm as the light source. Hydrogen production was analyzed using a gas chromatography-thermal conductivity detector (TCD), and AQY was calculated using the formula: AQY (%) = (number of produced H_2 molecules × 2/number of incident photons) × 100.

Acknowledgements

This work is financially supported by the Hainan Province Natural Science Foundation of China (220RC459) and National Natural Science Foundation of China (No. 22161016 and 22161017).

Conflict of Interests

The authors declare no conflict of interest.

Data Availability Statement

The data that support the findings of this study are available from the corresponding author upon reasonable request.

Keywords: calcination · organic-inorganic hybrid semiconductors · photocatalytic hydrogen production · sol-gel method · TiO_2

[1] a) C. Hu, X. Chen, Q. Dai, M. Wang, L. Qu, L. Dai, *Nano Energy* **2017**, *41*, 367–376; b) P. Thollander, J. Palm, J. Hedbrant, *Sustainability* **2019**, *11*, 1569; c) D. Tang, G.-L. Tan, G.-W. Li, J.-G. Liang, S. M. Ahmad, A. Bahadur, M. Humayun, H. Ullah, A. Khan, M. Bououdina, *J. Energy Storage* **2023**, *64*, 107196.
[2] a) L. Bertoluzzi, L. Badia-Bou, F. Fabregat-Santiago, S. Gimenez, J. Bisquert, *J. Phys. Chem. Lett.* **2013**, *4*, 1334–1339; b) G. Lazaroiu, E. Pop, G. Negreanu, I. Pisa, L. Mihaescu, A. Bondrea, V. Berbece, *Energy* **2017**, *127*, 351–357; c) T. Takata, K. Domen, *ACS Energy Lett.* **2019**, *4*, 542–549; d) M. Liu, Z. Yao, J. Gu, C. Li, X. Huang, L. Zhang, Z. Huang, M. Fan, *Chem. Eng. J.* **2023**, *461*, 141918.
[3] a) M. Ni, M. K. H. Leung, D. Y. C. Leung, K. Sumathy, *Renewable Sustainable Energy Rev.* **2007**, *11*, 401–425; b) M. Nasr, C. Eid, R. Habchi, P. Miele, M. Bechelany, *ChemSusChem* **2018**, *11*, 3023–3047.
[4] a) J. P. Jeon, D. H. Kweon, B. J. Jang, M. J. Ju, J. B. Baek, *Advanced Sustainable Systems* **2020**, *4*, 2000197; b) R. Li, T. Li, Q. Zhou, *Catalysts* **2020**, *10*, 804; c) X. Luo, W. Lai, X. Liu, *ChemistrySelect* **2021**, *6*, 39–46; d) W. Fang, M. Xing, J. Zhang, *Journal of Photochemistry and Photobiology C: Photochemistry Reviews* **2017**, *32*, 21–39; e) X. Liu, G. Zhu, X. Wang, X. Yuan, T. Lin, F. Huang, *Adv. Energy Mater.* **2016**, *6*, 1600452; f) M. Ghorbanloo, A. A. Nada, H. H. El-Maghrabi, M. F. Bekheet, W. Riedel, R. Viter, S. Roualdes, P. Miele, M. Bechelany, *J. Alloys Compd.* **2023**, *945*.
[5] a) M. Szkoda, K. Trzcinski, Z. Zarach, D. Roda, M. Lapinski, A. P. Nowak, *Materials (Basel)* **2021**, *14*, 5686; b) Y. Liang, S. Sun, T. Deng, H. Ding, W. Chen, Y. Chen, *Materials (Basel)* **2018**, *11*, 450; c) P. Su, M. Zhou, X. Lu, W. Yang, G. Ren, J. Cai, *Appl. Catal. B* **2019**, *245*, 583–595; d) A. A. Nada, M. F. Bekheet, R. Viter, P. Miele, S. Roualdes, M. Bechelany, *Appl. Catal. B* **2019**, *251*, 76–86.
[6] a) M. Ismael, *Fuel* **2021**, *303*, 121207; b) E. Coy, I. Iatsunskyi, M. Bechelany, *Solar RRL* **2023**, *7*.
[7] a) A. Wei, L. Chang, S. Luo, S. Cao, X. Bi, W. Yang, J. Liu, F. Zhang, *Ionics* **2021**, *28*, 555–565; b) K. Sumida, K. Liang, J. Reboul, I. A. Ibarra, S. Furukawa, P. Falcaro, *Chem. Mater.* **2017**, *29*, 2626–2645; c) H. Zhang, L. Xu, B. Han, H. Wang, Y. Liu, P. Wang, P. Lin, X. Wu, X. Yu, C. Cui, *J. Alloys Compd.* **2023**, *957*, 170394.
[8] a) X. Zeng, Y. Liu, X. Hu, X. Zhang, *Green Chem.* **2021**, *23*, 1466–1494; b) P. Bhavani, M. Hussain, Y.-K. Park, *J. Cleaner Prod.* **2022**, *330*, 129899; c) M. R. Geraskina, A. S. Dutton, M. J. Juetten, S. A. Wood, A. H. Winter, *Angew. Chem. Int. Ed. Engl.* **2017**, *56*, 9435–9439.
[9] a) Q. Ma, Y. Yu, M. Sindoro, A. G. Fane, R. Wang, H. Zhang, *Adv. Mater.* **2017**, *29*, 1605361; b) D. L. Ashford, M. K. Gish, A. K. Vannucci, M. K. Brennaman, J. L. Templeton, J. M. Papanikolas, T. J. Meyer, *Chem. Rev.* **2015**, *115*, 13006–13049; c) X. Xu, X. Wang, J. Shao, L. Hong, H. Zhang, S. Chu, *Int. J. Hydrogen Energy* **2023**, *48*, **15967–15974**.
[10] a) S.-H. Nam, T. K. Kim, J.-H. Boo, *Catal. Today* **2012**, *185*, 259–262; b) L. Szatmáry, S. Bakardjieva, J. Šubrt, P. Bezdička, J. Jirkovský, Z. Bastl, V. Brezová, M. Korenko, *Catal. Today* **2011**, *161*, 23–28; c) Y.-F. Chen, J.-F. Huang, M.-H. Shen, J.-M. Liu, L.-B. Huang, Y.-H. Zhong, S. Qin, J. Guo, C.-Y. Su, *J. Mater. Chem. A* **2019**, *7*, 19852–19861; d) M. Zhou, X. Zhong, D. Wei, K. Yang, Y. Chen, C. Jia, J. Li, *Green Chem.* **2022**, *24*, 2557–2566.
[11] a) Q. Lv, X. Ren, L. Liu, W. Guan, A. Liu, *Ionics* **2019**, *26*, 1325–1336; b) F. Jing, Y. Guo, B. Li, Y.-F. Chen, C. Jia, J. Li, *Chin. Chem. Lett.* **2022**, *33*, 1303–1307.
[12] J. Arun, S. Nachiappan, G. Rangarajan, R. P. Alagappan, K. P. Gopinath, E. Lichtfouse, *Environ. Chem. Lett.* **2023**, *21*, 339–362.

[13] S. Sakthivel, H. Kisch, *Angew. Chem. Int. Ed. Engl.* **2003**, *42*, 4908–4911.
[14] Z. Li, C. Wang, Z. Su, W. Zhang, N. Wang, G. Mele, J. Li, *Mater. Chem. Phys.* **2020**, *252*, 123228.
[15] M.-m. Yu, J. Li, W.-j. Sun, M. Jiang, F.-x. Zhang, *J. Mater. Sci.* **2014**, *49*, 5519–5528.
[16] a) J.-H. Xu, J. Li, W.-L. Dai, Y. Cao, H. Li, K. Fan, *Appl. Catal. B* **2008**, *79*, 72–80; b) M. Ghorbanloo, A. A. Nada, H. H. El-Maghrabi, M. F. Bekheet, W. Riedel, B. Djamel, R. Viter, S. Roualdes, F. S. Soliman, Y. M. Moustafa, P. Miele, M. Bechelany, *Appl. Surf. Sci.* **2022**, *594*.
[17] M. Wang, S. Su, X. Zhong, D. Kong, B. Li, Y. Song, C. Jia, Y. Chen, *Nanomaterials* **2022**, *12*, 1918.
[18] a) H. Wu, M. Wang, F. Jing, D. Kong, Y. Chen, C. Jia, J. Li, *Chin. Chem. Lett.* **2022**, *33*, 1983–1987; b) V. Kumaravel, S. Mathew, J. Bartlett, S. C. Pillai, *Appl. Catal. B* **2019**, *244*, 1021–1064; c) M. A. Barros, C. L. Seabra, M. J. Sampaio, C. Nunes, C. G. Silva, S. Reis, J. L. Faria, *Appl. Surf. Sci.* **2023**, *629*, 157311.
[19] a) A. Meng, L. Zhang, B. Cheng, J. Yu, *Adv. Mater.* **2019**, *31*, 1807660; b) Y.-H. Li, J.-Y. Li, Y.-J. Xu, *EnergyChem* **2021**, *3*,100047; c) J. Li, Y. Wu, L. Liu, R. L. Peng, J. Xu, J. He, H. Guo, *J. Alloys Compd.* **2023**, *957*, 170404; d) Z. Ren, M. Yu, H. Zhou, S. Yan, S. Hu, M. Xu, *Appl. Surf. Sci.* **2023**, *629*, 157328.
[20] T.-W. Jiang, X. Qin, K. Ye, W.-Y. Zhang, H. Li, W. Liu, S. Huo, X.-G. Zhang, K. Jiang, W.-B. Cai, *Appl. Catal. B* **2023**, *334*, 122815.
[21] B. Jana, D. Pan, N. Parshi, S. Maity, S. Das, J. Ganguly, *Mater. Chem. Phys.* **2022**, *282*, 125982.
[22] Q. Guo, C. Zhou, Z. Ma, X. Yang, *Adv. Mater.* **2019**, *31*, 1901997.
[23] a) M. Cai, R. Li, Z. Xie, J. Huang, Y. Zeng, Q. Zhang, H. Liu, W. Lv, G. Liu, *Appl. Catal. B* **2019**, *259*; b) J. Liu, J. Wan, L. Liu, W. Yang, J. Low, X. Gao, F. Fu, *Chem. Eng. J.* **2022**, *430*.

Manuscript received: April 6, 2023
Revised manuscript received: May 22, 2023
Accepted manuscript online: May 29, 2023

RESEARCH ARTICLE

The extensive π system in the naphthalene structure and the carboxylic acid group of 1,4-naphthalene dicarboxylic acid (NA) render it an exceptional organic semiconductor for doping TiO_2 using a calcination-free sol-gel method. The resulting catalyst exhibited a significantly improved hydrogen production rate by photolyzing water molecules under visible light, outperforming the efficiency of the calcined material.

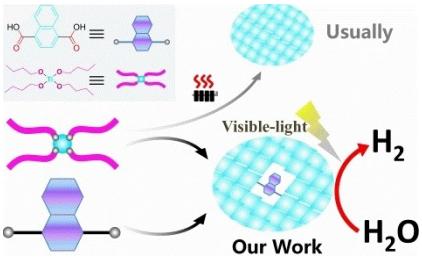

K. Yang, D. Wei, Prof. C. Jia, Dr. J. Li**

1 – 9

A Calcination-Free Sol-Gel Method to Prepare TiO_2-Based Hybrid Semiconductors for Enhanced Visible Light-Driven Hydrogen Production